Quaternary Science Reviews 29 (2010) 324–337

Contents lists available at ScienceDirect

Quaternary Science Reviews

journal homepage: www.elsevier.com/locate/quascirev

Atmospheric decadal variability from high-resolution Dome C ice core records of aerosol constituents beyond the Last Interglacial

Matthias Bigler [a,b,c,*], Regine Röthlisberger [d], Fabrice Lambert [a,b], Eric W. Wolff [d], Emiliano Castellano [e], Roberto Udisti [e], Thomas F. Stocker [a,b], Hubertus Fischer [a,b]

[a] Climate and Environmental Physics, Physics Institute, University of Bern, Sidlerstrasse 5, 3012 Bern, Switzerland
[b] Oeschger Centre for Climate Change Research, University of Bern, Bern, Switzerland
[c] Centre for Ice and Climate, Niels Bohr Institute, University of Copenhagen, Juliane Maries Vej 30, 2100 Copenhagen, Denmark
[d] British Antarctic Survey, Natural Environment Research Council, High Cross, Madingley Road, Cambridge CB3 0ET, UK
[e] Department of Chemistry, University of Florence, Via della Lastruccia 3, 50019 Sesto Fiorentino, Italy

ARTICLE INFO

Article history:
Received 9 February 2009
Received in revised form
1 September 2009
Accepted 4 September 2009

ABSTRACT

Along the EPICA Dome C ice core, we measured concentrations of different water-soluble aerosol constituents and deduced total depositional flux records. Here we present high-resolution sodium, calcium, ammonium and nitrate data covering the last 173,000 years. The first three of these species are passive tracers and reveal source and long-range transport changes whereas nitrate is deposited reversibly. However, it can be used to check isotope-derived accumulation rate estimates, a prerequisite to calculate total depositional fluxes. During the last two transitions from glacial to interglacial periods, changes in the total depositional flux differ strongly for different aerosol species. The largest changes are observed in the terrestrial aerosol proxy non-sea salt calcium, only moderate changes occur in the marine sea salt indicator sodium, while ammonium, a proxy for marine bioproductivity, remains rather constant. In agreement with previous studies, we find that only considerable glacial–interglacial changes at both, the terrestrial and the marine sea salt aerosol source can explain the observed pronounced changes. The unprecedented high-resolution of our data allows for the first time the examination of decadal variability back to the penultimate glacial period. On the one hand, we find occasional fast shifts occurring within a few years; here we present such an event in the calcium record from the penultimate glacial period. On the other hand, we examine variation coefficients and pairwise correlation coefficients, both determined in 200-year windows. They generally reveal only moderate changes. During glacial periods, slightly lower variation coefficients are found, concurrent with slightly higher correlation coefficients, which points to a more uniform and stronger coupled atmospheric long-range transport of the different aerosol species to the East Antarctic Plateau and less influence of cyclonic activities during cold periods. The opposite is observed for interglacial periods with probably even reinforced importance of cyclonic influences during the Last Interglacial period, the Marine Isotope Stage 5.5. This period reveals no evidence for abrupt climatic changes in any of the species, however, the marine sea salt aerosol indicator sodium shows a distinct minimum followed by a pronounced increase. This pattern is explained by significantly reduced sea ice production in the Indian Southern Ocean sector, which is believed to be the dominant source of sodium deposited in Dome C during warm periods.

1. Introduction

1.1. Atmospheric circulation over glacial and interglacial periods

The centred position of Antarctica around Earth's South Pole and the lack of significant landmasses in a broad longitudinal band enable a well-developed westerly circulation, driven primarily by strong pole-equator sea level pressure gradients (King and Turner, 1997). It shows a present-day near-surface wind maximum at

* Corresponding author at: Climate and Environmental Physics, Physics Institute, University of Bern, Sidlerstrasse 5, 3012 Bern, Switzerland. Tel.: +41 (0)31 631 8673; fax: +41 (0)31 631 8742.
E-mail addresses: bigler@climate.unibe.ch (M. Bigler), regine.rothlisberger@googlemail.com (R. Röthlisberger), lambert@climate.unibe.ch (F. Lambert), ewwo@bas.ac.uk (E.W. Wolff), emiliano.castellano@unifi.it (E. Castellano), udisti@unifi.it (R. Udisti), stocker@climate.unibe.ch (T.F. Stocker), hfischer@climate.unibe.ch (H. Fischer).

0277-3791/$ – see front matter © 2009 Elsevier Ltd. All rights reserved.
doi:10.1016/j.quascirev.2009.09.009

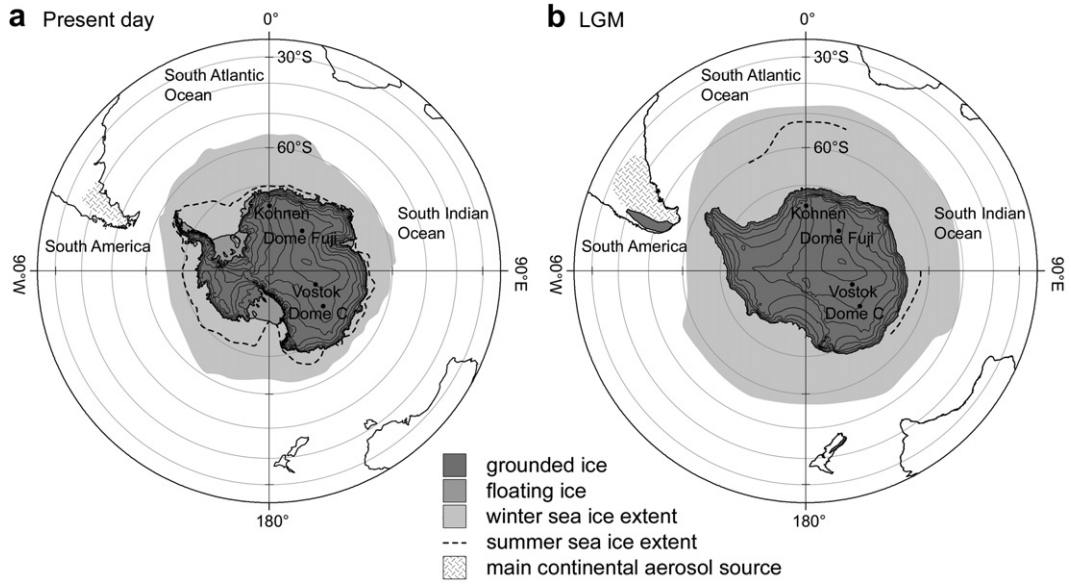

Fig. 1. Antarctica with the deep ice core drill site Dome C (among others) and the surrounding southern hemisphere for (a) present-day and (b) LGM. Ice sheets (with 500 m height contour lines) and coast lines are according to Huybrechts (2009), winter and summer sea ice extent from Gersonde et al. (2005). The potential southern South American (SSA) source region of terrestrial aerosol to East Antarctica is hatched (Iriondo, 2000).

around 50°S leading to the Antarctic circumpolar ocean surface current (Shulmeister et al., 2004). An important mode of pressure variation in the westerly circulation is the Antarctic Annular Oscillation (AAO)[1] (Thompson and Wallace, 2000). It is mainly considered sub-decadal, but exists also on decadal and longer time scales (Simmonds, 2003; Shulmeister et al., 2004), and it seems to be connected to the interannual variation of storm tracks in the Southern Hemisphere (Rao et al., 2003). These cyclonic activities play an important role in the atmosphere–ocean–sea–ice-interactions and the poleward transport of heat and moisture (Simmonds, 2003).

Over glacial–interglacial cycles, topographic conditions (Fig. 1), such as extent and shape of the Antarctic ice sheet and exposed continental shelves (due to the lower sea level), did not change very much (Huybrechts, 2009). In contrast, glacial–interglacial winter and summer sea ice extent varied markedly, though, in the Indian sector of the Southern Ocean (SO) mainly the winter extent (Gersonde et al., 2005). However, the general circulation pattern in terms of atmospheric transport paths and transport times most likely did not change fundamentally: Shulmeister et al. (2004) examined past westerly circulation patterns in the Australian sector of the SO based on different terrestrial and marine records and found evidence of some strengthening during the Last Glacial Maximum (LGM), followed by some weakening in the early Holocene and a return to stronger circulation afterwards. In contrast, South American proxy data lead to inconsistent conclusions regarding position and strength of the westerlies at the LGM in this sector of the SO (Wolff et al., 2010, and references therein). Modelling results of aerosol transport support the assumption that changes in the meridional transport were only moderate between LGM and Holocene, however, again showing somewhat inconsistent results. While Lunt and Valdes (2001) find a lower transport efficiency and small interannual variations during the LGM compared to present-day (based on analysis of back trajectories initialized in Dome C), Krinner and Genthon (2003) state that long-range transport occurred preferentially in the mid-troposphere and was slightly faster during the LGM (based on general circulation model simulations). Yet, both models simplify deposition processes during transport, as they consider solely dry deposition of aerosols en route. Based on the joint use of ice core data from opposite sites of East Antarctica and a simple conceptual transport model, Fischer et al. (2007b) found that transport effects accounted for maximal a factor of two changes in aerosol fluxes between glacial and interglacial periods with most of the effect due to the change in precipitation, hence, wet deposition en route.

1.2. Marine Isotope Stage 5.5

The characterization of the Last Interglacial period along with the related transitions is of great interest (Broecker and Henderson, 1998), as it is often used as an analogue for a possible warmer future climate. It corresponds to Marine Isotope Stage (MIS) 5.5, approximately simultaneous to the Eemian period in European Pleistocene stratigraphy. The onset of MIS 5.5 has been defined as the stratigraphic limit between the Middle and the Upper Pleistocene (Gibbard, 2003). Although other interglacial periods may show a greater similarity to the Holocene in terms of their orbital parameters (Loutre and Berger, 2003), the MIS 5.5 plays a key role in paleoclimatology due to better availability and resolution of different records (van Kolfschoten et al., 2003). However, data covering MIS 5.5 are still not abundant enough to draw a complete picture, especially for southern high latitude areas, a region which acts as an important player in global climate change involving different feedback mechanisms. Global model simulations together with local paleorecords suggest that MIS 5.5 was on average warmer compared to the modern preindustrial climate (Jansen et al., 2007), while relative sea levels were at least 3 m above the present level (Stirling et al., 1998). In Antarctica, the temperature offset was probably even higher (Overpeck et al., 2006), especially during the early MIS 5.5, estimated to be +4.5 °C based on water isotope measurements on the Dome C ice core (Jouzel et al., 2007). Of particular interest are investigations whether the MIS 5.5 climate was smooth (like the Holocene) or experienced abrupt

[1] Also referred to as High-Latitude Mode (HLM) or Southern Annular Mode (SMA).

cooling events as indicated in marine sediment records from the SO (Ninnemann et al., 1999; Bianchi and Gersonde, 2002); moreover, if there is evidence for an Antarctic cold reversal-like event during Termination II into MIS 5.5, which would be the counterpart of a Younger Dryas-like event as found in some stratigraphic records from the Northern Hemisphere (e.g. Sánchez Goñi et al., 1999).

1.3. Scope of this study

Reconstructions of glacial–interglacial and millennial-scale changes in terrestrial and sea salt aerosol emission, transport and deposition to East Antarctica have been carried out, e.g. by Röthlisberger et al. (2002a), Wolff et al. (2006), including nssSO_4^{2-}, a tracer related to marine bioproductivity, Fischer et al. (2007a,b), and Lambert et al. (2008), the latter with respect to water-insoluble mineral dust particles. In a recent study, Röthlisberger et al. (2008) additionally examined glacial–interglacial terminations in detail. Here we aim at complementing the picture by examining for the first time the decadal variations considering high-resolution ice core records of aerosol constituents from Dome C, namely sodium (Na^+), calcium (Ca^{2+}) and ammonium (NH_4^+), which are all irreversibly deposited passive tracers. Their use as climatic proxies is described in the following part of the introduction.

1.4. Sea salt aerosol

An obvious proxy for sea salt aerosol is the water-soluble sodium ion (Na^+), but since Na^+ also has terrestrial sources, it is more appropriate to use calculated sea salt sodium (ssNa^+), especially during glacial periods, where the atmospheric load of terrestrial aerosol was high. Seasonal maxima of the present-day Na^+ deposition onto the Antarctic ice sheet are observed in winter and spring (Sommer et al., 2000; Hara et al., 2004; Weller and Wagenbach, 2007) when the sea ice extent is largest and the open ocean is furthest away. As the source of sea salt aerosol is usually attributed to the open ocean, where it is formed by wind-induced bubble bursting of breaking waves, this would require a strongly enhanced meridional transport during winter which is neither observed nor supported by models in such a degree (Section 1.1). Therefore, an alternative mechanism was proposed, where sea salt aerosol production is related to sea ice processes, such as brine and frost flower formation (on freshly formed or submerged sea ice) and blowing snow (Wagenbach et al., 1998; Rankin et al., 2000; Wolff et al., 2003; Yang et al., 2008), thus linking the deposition of sea salt aerosol onto the ice sheet to the sea ice production rate. The two different sources can be distinguished, as the open ocean source causes no significant fractionation regarding the ionic composition of sea water, whereas the sea ice related process is accompanied by significant SO_4^{2-} and, to a lesser extent, Na^+ depletion due to mirabilite precipitation at low temperatures. Indeed, such depletion events have been reported also for the East Antarctic plateau (Hara et al., 2004; Jourdain et al., 2008), however, the quantitative contribution to the ssNa^+ deposition at these sites remains still unclear (Bigler et al., 2006), as a non-linear relationship between ssNa^+ and sea ice extent is expected. Additionally, it has been shown that ssNa^+ fails as a quantitative proxy for sea ice extent during glacial periods (Fischer et al., 2007b; Röthlisberger et al., 2008; Röthlisberger et al., 2010) because it becomes increasingly insensitive to the glacial expansion of sea ice due to the increased transport time for sea salt aerosol to reach the high East Antarctic plateau. Thus, we interpret ssNa^+ here as a sea salt proxy which is influenced by both possible source processes, however restricted to the closest source area, the Indian sector of the SO, as indicated by back trajectory calculations (Reijmer et al., 2002) and by the limited atmospheric lifetime of the sea salt aerosol (Fischer et al., 2007b; Röthlisberger et al., 2010).

1.5. Terrestrial aerosol

Southern South America (SSA) is in a distinct position as southernmost continental landmass. Based on geochemical evidence (strontium and neodymium isotope ratios) and modelling results, it is believed to be the most important supplier of glacial terrestrial aerosols to Antarctica (Gaiero, 2007; Delmonte et al., 2008), whereas Australia may also play a significant role during interglacial periods (Revel-Rolland et al., 2006 and references therein; Li et al., 2008). Therefore, ice core records of the terrestrial aerosol flux are related to the evolution of the SSA climate during glacial periods, whereas for interglacial periods such a clear attribution is not possible. In contrast to sea salt aerosol, the terrestrial aerosol source rather has the characteristic of a point source, or better a set of point sources. Even within one main source area, such as SSA, different sub regions can contribute, like Patagonia or the Puna-Altiplano plateau (Delmonte et al., 2010; Gaiero, 2007). High surface wind speeds, vegetation cover, soil texture and humidity, and chemical and physical weathering are important factors to produce terrestrial aerosols. Sugden et al. (2009) for instance found, that Antarctic dust peaks can be related to periods with glacial melt water deposition onto outwash plains in Patagonia, whereas dust availability may be reduced when the glaciers end in pro-glacial lakes. Again, the prevailing transport between the source regions and the ice sheet is included as well in the terrestrial aerosol ice core signal. Apart from water-insoluble mineral dust particles (e.g. Delmonte et al., 2002; Lambert et al., 2008) the water-soluble calcium ion (Ca^{2+}) is an ice core proxy for terrestrial aerosol. However, in some cases the contribution of Ca^{2+} from sea water has to be deducted by calculating non-sea salt calcium (nssCa^{2+}), especially during interglacial periods, where the terrestrial aerosol load of the atmosphere is rather low compared to the sea salt contribution. Seasonal maxima of the present-day Ca^{2+} deposition onto the ice sheet are observed in winter (Whitlow et al., 1992; Sommer et al., 2000). In summary, nssCa^{2+} from East Antarctic ice cores is a valuable proxy for SSA climate and environment in glacial periods, yet, its interpretation for interglacial periods is not straightforward.

1.6. Marine bioproductivity

Marine biogenic emissions can be examined based on different proxies in East Antarctic ice cores (Wolff et al., 2006; Kaufmann et al., 2010). Here we focus on the irreversibly deposited water-soluble ammonium (NH_4^+) ion (Silvente and Legrand, 1993; Legrand et al., 1999). The emission of ammonia (NH_3) related to natural biogenic production in marine environments (Johnson and Bell, 2008) is followed by neutralization with mainly sulphuric acid resulting in ammonium sulphate. Therefore, NH_4^+ develops from secondary aerosol processes involving gas-to-particle conversion and transport of sub-micrometric particles. From coastal Antarctic stations it is known that summer maxima of NH_4^+ coincide with peaks of non-sea salt sulphate (nssSO_4^{2-}) originating from remote marine biogenic emissions of dimethyl sulphide (DMS; Legrand et al., 1998, 1999). The summer peak of both, NH_4^+ and nssSO_4^{2-} is also observed further inland on the plateau (Kohnen), probably slightly earlier for NH_4^+ (Sommer et al., 2000; Weller and Wagenbach, 2007). Modelling results point to a present-day mean source of nssSO_4^{2-} for the East Antarctic plateau (Vostok) at around 55–65°S (Cosme et al., 2005), however, for NH_4^+ it is presumably located even further north (Kaufmann et al., 2010). Thus, we assume the small amount of NH_4^+ deposited on the East Antarctic

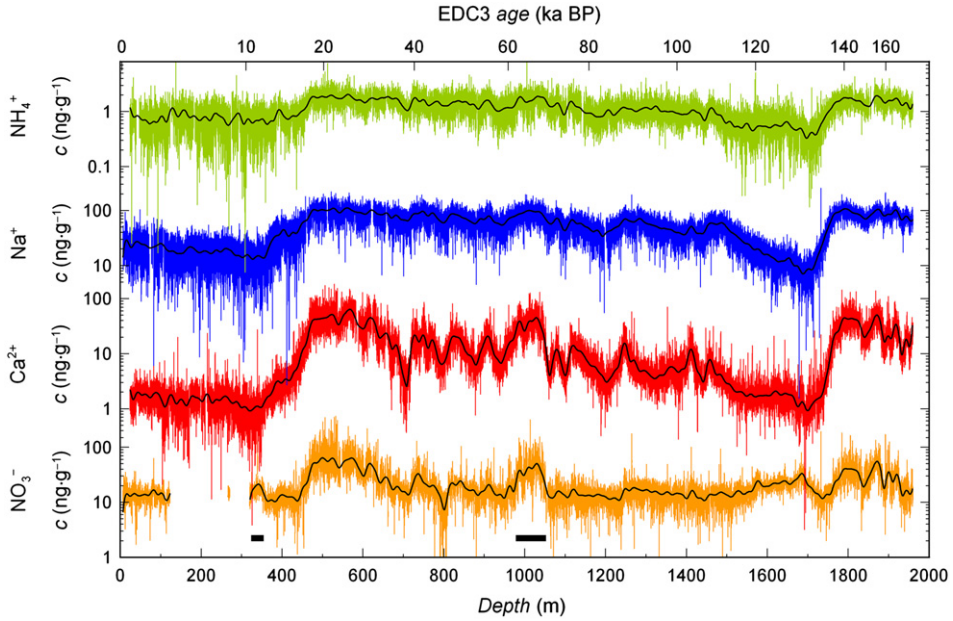

Fig. 2. Continuous high-resolution records of NH_4^+, Na^+, Ca^{2+} and NO_3^- concentrations c (on log axes) in 0.5 cm sampling resolution (thin lines) and low-pass filtered with a 20 m cutoff length (thick black lines) from the EPICA Dome C ice core down to 1960 m depth and covering the time span back to approximately 173 ka BP. The two horizontal bars highlight NO_3^- maxima discussed in Section 3.1.

plateau to be derived from marine biogenic production in the seasonal sea ice zone and further north in the SO.

2. Data and methods

2.1. Data acquisition, performance and dating

In the frame of the European Project for Ice Coring in Antarctica (EPICA) several field campaigns have been carried out at Concordia Station between 1995 and 2005 to retrieve a deep ice core reaching as far back in time as possible (EPICA community members, 2004). The 3260 m long core is around 800,000 years old at a depth of 3200 m; below it is apparently subject to anomalous flow, preventing an unambiguous age assignment (Jouzel et al., 2007). It is denoted EDC ice core and consists of two parts, EDC96 and EDC99, because the drilling had to be restarted after the drill got stuck in 1999. The Dome C drill site is located on the East Antarctic Plateau at 75°06′S, 123°21′E and 3233 m above sea level, at least ~1100 km away from the coast (Fig. 1). The site is characterised by a mean annual surface temperature of −54.5 °C and a present-day accumulation rate of 25 kg m^{-2} a^{-1}.

Apart from drilling, some analyses were performed already in the field, e.g. measurements of the water-soluble ion mass concentrations c (in ng g^{-1} or ppbw) of sodium (Na^+), calcium (Ca^{2+}), ammonium (NH_4^+), nitrate (NO_3^-) and other aerosol constituents. For this, a continuous flow analysis (CFA) system was used which produces high-resolution c data with a sampling resolution of 0.5 cm or less (Röthlisberger et al., 2000b; Kaufmann et al., 2008).[2] Because of signal dispersion in the CFA system, the effective depth resolution is found to be between 1 cm and 1.5 cm for the different aerosol species (Bigler et al., 2006). Measurement errors are estimated to be generally below 10% (Röthlisberger et al., 2000b). Limits of detection (LOD, defined as three times the standard deviation of blank measurements) are 3 ng g^{-1} for Na^+, 0.2 ng g^{-1} for Ca^{2+}, 0.1 ng g^{-1} for NH_4^+ and 2 ng g^{-1} for NO_3^-, respectively. Especially for Ca^{2+} and NH_4^+ this is one order of magnitude better than what can be typically achieved in discrete ion chromatography (IC) measurements. Thus, for NH_4^+ CFA represents the only technique to derive reliable ice core records from Antarctica. In the case of Ca^{2+} it provides reliable data also from interglacial ice where concentrations are too low to obtain good data by the standard IC method (Littot et al., 2002; Wolff et al., 2006). In this study we use only CFA data although samples for IC and FIC (fast IC) were taken in parallel and analyzed subsequently (Wolff et al., 2006, 2010). Yet, their resolution is not sufficient enough and the combination of the data sets achieved by different laboratories was quite difficult in order to use them for decadal-resolution studies.

For the age determination of the ice, the EDC3 timescale was used (Parrenin et al., 2007a,b). Ages are given in 1000 years before present (ka BP) whereas 0 ka BP corresponds to 1950 AD. Maximal age uncertainties are 1 ka at 18 ka BP (LGM), 3 ka at 100 ka BP and 6 ka at 130 ka BP (Parrenin et al., 2007b). Time markers used in this study to distinguish between glacial, interglacial and transition periods are based on distinctive features of our data and the deuterium isotope record (δD), a proxy for the temperature at the drill site (Jouzel et al., 2007). They are not claimed to be stratigraphic markers in a narrow sense. Applying the EDC3 time scale to both cores, EDC96 and EDC99, results in a little inhomogeneity in the short, overlapping part, as both cores have their own depth scale. Thus, they have been aligned in a way that the peak patterns match on the common EDC3 timescale.

As we aim at discussing decadal variability in this study, we only consider data down to the depth of 1960 m (~173 ka BP) within the penultimate glacial period and thus including two warm periods (the Holocene and the MIS 5.5), two glacial maxima (the Last Glacial Maximum (LGM) and MIS 6), three transitions (Termination I between LGM and Holocene, Termination II and glacial Inception I, both framing MIS 5.5) and several Antarctic isotope maxima (AIM; according to EPICA community members, 2006; Fischer et al.,

[2] The ice from 585 m to 788 m depth and below 3139 m was measured by the Bern CFA at the Alfred Wegener Institute in Bremerhaven, Germany.

2007b). Fig. 2 gives an overview of the high-resolution c records on the depth scale. To highlight general features, we added a low-pass filtered version to the figure (finite impulse response (FIR) on an 80 m Hamming window with a 20 m cutoff length). Additionally, a detailed section is shown in Fig. 3 from around 1832 m depth (~148 ka BP) to emphasise the high-resolution of our data.

2.2. Data treatment and representation

By linearly interpolating between the given depth-age points of the coarser resolved EDC3 timescale we calculated annual mean c values from the high-resolution CFA data. Considering the analytical depth resolution of our measurements, the very low accumulation rate and post-depositional reworking of snow surface layers, annual layers are not preserved at the site. Thus, the calculated annual means have only a formal character. To account for the least resolved data used in this study (i.e. between approximately 1750 m and 1960 m depth), we applied a low-pass filter (FIR on a 31 year Hamming window) with a 10 year cutoff period. Previously, we interpolated data gaps up to 3 years length. By this interpolation and filtering procedure we achieved a homogenous decadal-resolution of all records over the whole depth range (hereafter denoted decadal-resolution data) allowing for proper variability comparisons back in time. In order to highlight long-term patterns, we finally also applied a low-pass filter with a 1 ka cutoff period (FIR on a 3 ka Hamming window).

Concentrations c are always positive but generally show an asymmetry towards large values; therefore, they are better represented by a log-normal than a normal distribution (Yiou et al., 1997; Castellano et al., 2004). Quantile–quantile-plots of our c data (Supplementary Fig. I) confirm this behaviour for different time intervals and different aerosol species. Therefore, we use exclusively log scales to present and discuss our data. However, mean $\bar{c}$ and variance $s_{\bar{c}}^2$ of $\log(c)$ data can be back-transformed to the median $\tilde{c}$ (which is more robust than the mean regarding outliers) and the variation coefficient ν_c in concentration units ng g^{-1}, respectively, to be more easily accessible; this applies similarly to total depositional fluxes f (see Section 2.3):

$$\tilde{c} = 10^{\bar{c}}; \quad \nu_c = \sqrt{10^{s_{\bar{c}}^2} - 1} \tag{1}$$

Based on decadal-resolution c data, $\tilde{c}$ from some distinguished periods are given in Table 1a.

Later in this study, variation coefficients ν (according to Eq. (1)) will be used to calculate the relative variability of the decadal-resolution data within 200-year windows. Similarly, correlations between different records (Na^+, Ca^{2+} and NH_4^+) within 200-year windows will be discussed using empirical linear correlation coefficients r (Pearson correlation). To test the significance of positive correlations r by a single-sided t-test, we have to account for the fact that the data points are not statistically independent and thus show some autocorrelation, e.g. due to the filtering procedure leading to decadal-resolution. Therefore, the effective number of data points n_{eff} is considerably smaller than the window size $n = 200$ and is calculated according to Quenouille (1952) by

$$n_{\text{eff}} = \frac{n}{1 + 2r_1r_1' + 2r_2r_2' + \cdots + 2r_kr_k'}, \tag{2}$$

where r_1 is the lag-1 autocorrelation of the one data series and r_1' is the lag-1 autocorrelation of the other data series; r_2 and r_2' are the corresponding lag-2 autocorrelations of both time series and so on to the maximal lag-k.

2.3. Reconstruction of atmospheric signals

Concentrations c can be directly measured in ice; however, they are not only influenced by the atmospheric aerosol load prior to the deposition. For sites where clear sky precipitation prevails and dry deposition is dominant, as it is the case in Dome C with its very low present-day and even lower glacial accumulation rate, the snow accumulation significantly dilutes dry aerosol deposition (Legrand, 1987; Wolff et al., 2006; Fischer et al., 2007a). Therefore, it is more appropriate to discuss total depositional fluxes f because they are more representative of initial atmospheric concentrations.

Accumulation rates result directly from the EDC3 timescale (Parrenin et al., 2007a,b) and are given in cm ice-equivalent per year in coarser resolution than CFA data. Hence, they had to be: (1) transformed to kg m^{-2} a^{-1} water-equivalent by using an ice density of 917 kg m^{-3}; and (2) linearly interpolated between given values. Multiplication with c then led to the total depositional flux f in μg

Table 1
(a) Mass concentration medians $\tilde{c}$ and variation coefficients ν_c, and (b) total depositional fluxes medians $\tilde{f}$ and variation coefficients ν_f calculated on the basis of decadal-resolution data in distinguished and stable time intervals Δt.

(a)							
Δt (ka)	Period	$\tilde{c}$ in ng g^{-1} (ν_c in %)					
		Ca^{2+}	$nssCa^{2+}$	Na^+	$ssNa^+$	NH_4^+	NO_3^-
0.0–3.0	Late Holocene	1.6 (18)	0.6 (64)	23 (16)	22 (16)	0.7 (19)	13 (16)
3.0–8.0	Mid Holocene	1.4 (19)	0.6 (55)	18 (17)	17 (18)	0.8 (19)	
10.0–11.5	Early Holocene	1.0 (22)	0.3 (66)	14 (15)	14 (15)	0.7 (19)	17 (17)
18.0–23.0	LGM	43 (18)	41 (19)	101 (12)	60 (23)	1.8 (13)	53 (25)
124–127	Mid MIS 5.5	1.7 (21)	1.2 (33)	12 (18)	11 (21)	0.6 (20)	23 (11)
128–130	Early MIS 5.5	1.0 (28)	0.7 (45)	7.6 (23)	6.6 (28)	0.4 (23)	
139–146	MIS 6	42 (17)	40 (18)	98 (11)	58 (24)	1.7 (12)	38 (22)
(b)							
Δt (ka)	Period	$\tilde{f}$ in μg m^{-2} a^{-1} (ν_f in %)					
		Ca^{2+}	$nssCa^{2+}$	Na^+	$ssNa^+$	NH_4^+	
0.0–3.0	Late Holocene	42 (18)	15 (64)	598 (15)	576 (16)	18 (19)	
3.0–8.0	Mid Holocene	37 (19)	15 (55)	461 (17)	443 (18)	21 (19)	
10.0–11.5	Early Holocene	30 (22)	11 (66)	421 (15)	409 (15)	20 (19)	
18.0–23.0	LGM	535 (18)	502 (19)	1246 (12)	740 (23)	23 (13)	
124–127	Mid MIS 5.5	53 (21)	37 (33)	359 (18)	319 (21)	17 (20)	
128–130	Early MIS 5.5	40 (29)	26 (46)	289 (23)	249 (28)	15 (23)	
139–146	MIS 6	541 (16)	508 (17)	1249 (10)	739 (24)	22 (12)	

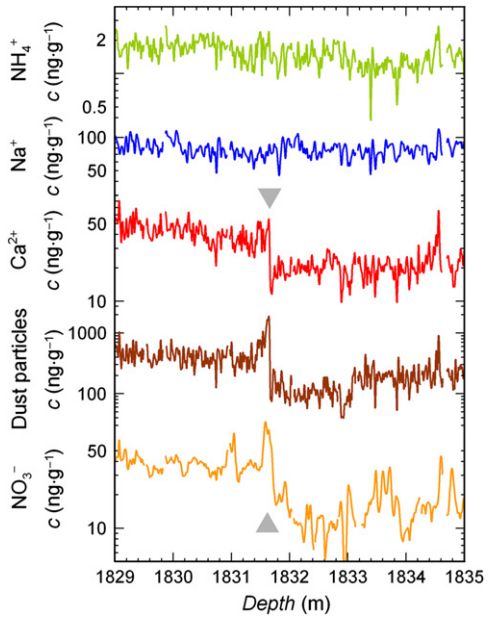

Fig. 3. Detailed section of the continuous high-resolution measurements of NH_4^+, Na^+, Ca^{2+}, NO_3^- and water-insoluble dust particle concentrations c (on log axes) in 0.5 cm sampling resolution from a 6 m depth interval around 148 ka BP. The shift in the Ca^{2+} and dust particle levels happens within 1 cm and is also reflected (more gradual) in the NO_3^- data. Na^+ and NH_4^+ show no significant shift at the same depth.

m^{-2} a^{-1}. Fig. 4 shows the calculated decadal-resolution and 1 ka cutoff, low-pass filtered f records of irreversibly deposited Ca^{2+}, Na^+ and NH_4^+ (but not NO_3^-, see Section 3.1) on the EDC3 timescale along with similarly filtered δD, reflecting changes of their sources and/or atmospheric transport to the drill site. Based on decadal-resolution f data, medians $\tilde{f}$ and variation coefficients v_f were calculated according to Eq. (1) (Section 2.2) for some distinguished and stable time intervals. They are given in Table 1b.

2.4. Reconstruction of source-separated signals

Both water-soluble ions, Na^+ and Ca^{2+}, have a marine and a terrestrial source. Based on our high-resolution Na^+ and Ca^{2+} data, mean ion mass ratios were deduced for water-soluble terrestrial and sea salt aerosol over East Antarctica in an earlier publication (Bigler et al., 2006). The resulting terrestrial ion mass ratio $(Na^+/Ca^{2+})_{nss} = 0.94$ points to a substantial role of halide terrestrial aerosols and is in agreement with the source properties of SSA. Thus, it is significantly higher than the elemental ratio of mean crust of 0.56 (Bowen, 1979) which has been used for source-separation in many previous ice core studies (although it includes also the water-insoluble fraction of dust and does not necessarily reflect the composition of the terrestrial aerosol from this very specific source region). In contrast, the resulting sea salt ion mass ratio $(Na^+/Ca^{2+})_{ss} = 23$ (Bigler et al., 2006) is in the range predicted for both, aerosol from wind-induced bubble bursting of breaking waves over the open ocean and sea ice brine derived aerosols, respectively. Based on these two ratios we calculate sea salt sodium ($ssNa^+$) and non-sea salt calcium ($nssCa^{2+}$) according to the equations given in Bigler et al. (2006). This procedure can, however, only be applied to coarser resolved, filtered data and not to the decadal-resolution records, as the ratios are mean values and may not apply on a short-term base. The calculations of decadal-resolution $ssNa^+$ and $nssCa^{2+}$ records would entail artificial variability and hence, mask the true signal variability. The results are shown in Fig. 5, along with uncorrected Na^+ and Ca^{2+} f records. Some figures of $\tilde{c}$ and $\tilde{f}$ derived from $ssNa^+$ and $nssCa^{2+}$ are given in Tables 1a,b,

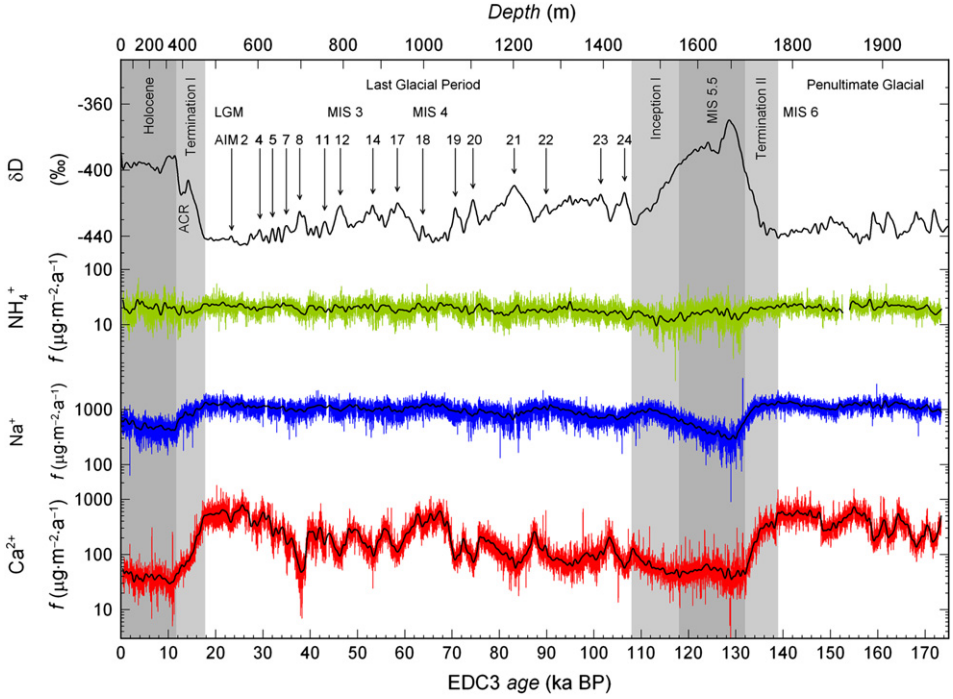

Fig. 4. Calculated records of the total depositional flux f (on log axes) of NH_4^+, Na^+ and Ca^{2+} on the Dome C ice core timescale EDC3. Decadal-resolution data (thin lines) were calculated from the high-resolution data in order to homogenize all data to the least resolved data at the deepest depth. A 1 ka cutoff low-pass filter was applied to show millennial variations (thick black lines). For comparison, the similarly filtered δD record (Jouzel et al., 2007) is shown as well. Denoted in the panel are the Antarctic cold reversal (ACR), the Last Glacial Maximum (LGM), some Marine Isotope Stages (MIS), the glacial maximum of the penultimate glacial period (MIS 6), and the Antarctic isotope maxima (EPICA community members, 2006; Fischer et al., 2007b).

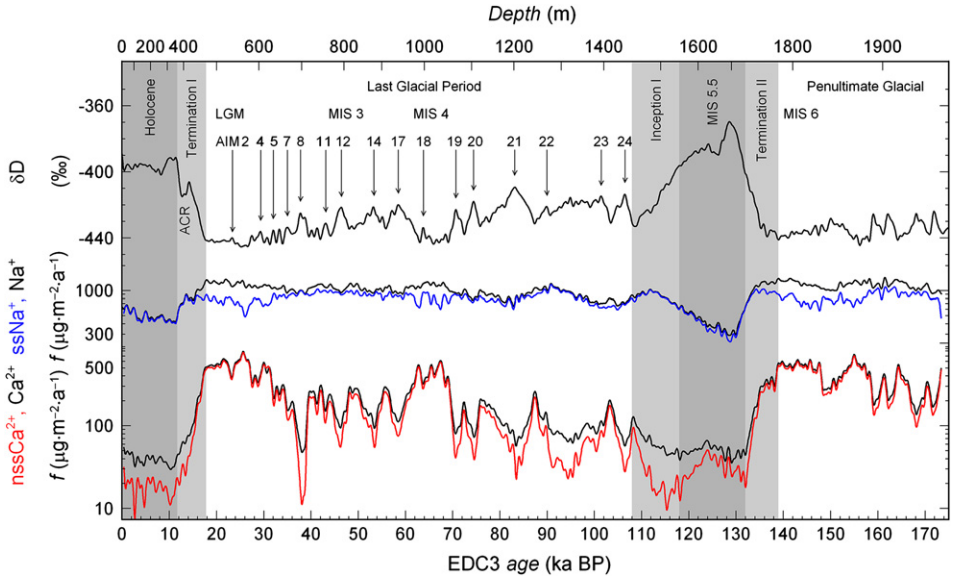

Fig. 5. Calculated source-separated records of the total depositional flux f (on log axes) of $ssNa^+$ (blue) and $nssCa^{2+}$ (red) low-pass filtered by a 1 ka cutoff filter. Filtered total Na^+ and Ca^{2+} records (black), δD, timescale, and labels are similar to Fig. 4.

respectively. From there, it is obvious that the source-separation has only significant effects for $ssNa^+$ during glacial maximum periods (where the decisive $(Na^+/Ca^{2+})_{nss}$ ratio is well defined) and for $nssCa^{2+}$ in interglacial periods (where $(Na^+/Ca^{2+})_{nss}$ is not well defined but insignificant for the correction). Errors, introduced by this separation, are likewise restricted to the corresponding periods.

3. Results

3.1. Interglacial accumulation rates reflected in the nitrate record

Nitrate NO_3^- (Figs. 2 and 3) is difficult to interpret because it is reversibly deposited. Ice concentrations c are strongly affected by the local temperature, accumulation rate and the coinciding terrestrial dust content (Röthlisberger et al., 2000a, b).

During cold glacial periods (e.g. 167–139 ka BP and 70–17 ka BP) c of NO_3^- and Ca^{2+} are co-varying on long-term timescales (Fig. 2), whereas in detail this co-variation is weaker (Fig. 3), pointing to a certain complexity of the governing processes. In general, lower temperatures and the reaction of NO_3^- with terrestrial dust aerosol (here represented by Ca^{2+}) reduce or prevent NO_3^- losses despite lower accumulation rates (Röthlisberger et al., 2000a). This leads to higher levels and higher variability during cold glacial periods. Such an increase in decadal variability during cold glacial periods is unique compared to the irreversibly deposited aerosol constituents (Ca^{2+}, Na^+ and NH_4^+) which show a slight decrease or remain constant (see Section 3.4 and Table 1a). Additionally, post-depositional dislocation of NO_3^- ions in the ice might be responsible for the weaker co-variation of the high-resolution data (Fig. 3) leading to more gradual shifts and misfits of single peaks. Despite similar Ca^{2+} levels (as well as similar local temperatures and accumulation rates), NO_3^- is significantly lower in MIS 6 than in the LGM. We speculate that this could indicate different NO_3^- source strengths. As main sources for central East Antarctica, stratospheric production, tropospheric lightning and organic origins are discussed (Röthlisberger et al., 2000a; Wolff et al., 2008).

During warm periods, when Ca^{2+} concentrations are low, accumulation rate and temperature control the NO_3^- preservation (Röthlisberger et al., 2000a). However, because the temperature difference between MIS 5.5 and Holocene (present-day mean annual surface temperature of −54.5 °C) probably did not exceed 2–4.5 °C (Jouzel et al., 2007), the temperature effect is assumed to be negligible and different NO_3^- levels are therefore qualitatively explained with effects related to the accumulation rate. NO_3^- c data (Fig. 2) are significantly higher during the whole MIS 5.5 compared to the available Holocene data, even the NO_3^- peak related to an accumulation rate maximum in the early Holocene does not reach MIS 5.5 values; a similar peak in the early MIS 5.5 reaches twice the value of the early Holocene. This result may be an independent, qualitative indication for higher accumulation rates during the whole MIS 5.5, in agreement with the commonly used δD-derived accumulation rates. This is further discussed and presented in Wolff et al. (2010) covering the warm periods of the last 800,000 years. The evaluation of our NO_3^- record revealed additionally, that due to the likely post-depositional dislocation of NO_3^- (as mentioned above), such accumulation rate estimates cannot be extended to high-resolution data and are only possible in coarse resolution. However, to estimate the accumulation rate quantitatively, the understanding of the air–snow-transfer of NO_3^- needs further improvements with regard to measurements and modelling (Röthlisberger et al., 2002b; Wolff et al., 2008). Although δD-derived accumulation rates have been questioned (Udisti et al., 2004; Wolff et al., 2010) and the error is estimated to be up to 30% during glacial periods (Schwander et al., 2001; Fischer et al., 2007b), it remains the best guess, especially regarding its availability over the whole data set.

Within Termination II (namely 135–130 ka BP), Inception I, the early last glacial period (namely 119–70 ka BP), and Termination I (namely 14.5–11.5 ka BP) our NO_3^- c data show minima: the terrestrial aerosol level is already low and the accumulation rate still low, so that NO_3^- losses are pronounced. In summary, the NO_3^- f record does not represent an unambiguous atmospheric signal and is not further considered in this study.

3.2. Measurements on a replicated ice core section

Within the overlap of the two EPICA Dome C ice cores, EDC96 and EDC99, located 10 m apart from each other, a section of ~17.4 m length was measured twice (Fig. 6a). These data can be

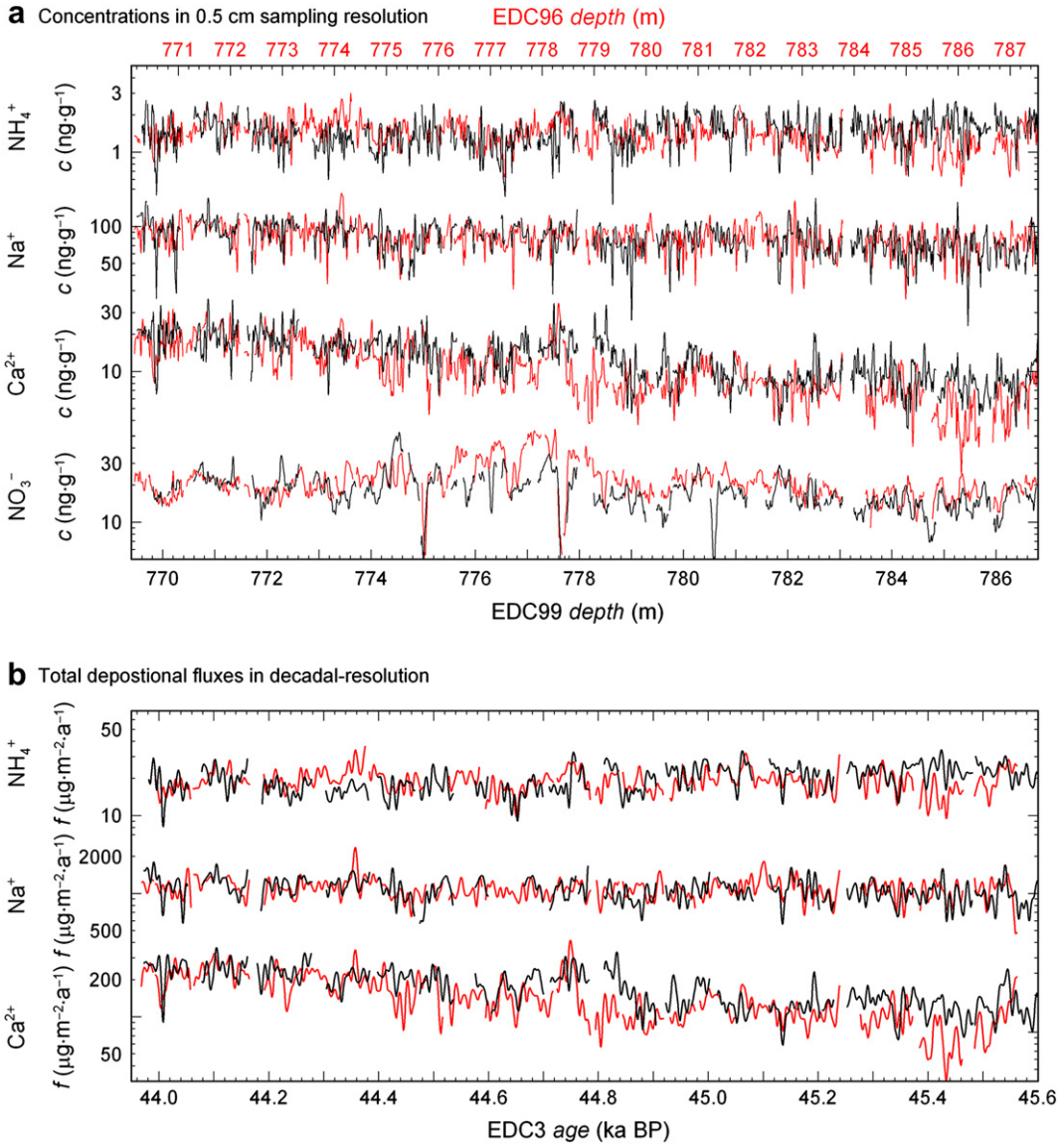

Fig. 6. Overlap of the EDC96 (red) and EDC99 (black) ice cores around 45 ka BP: (a) High-resolution records of NH_4^+, Na^+, Ca^{2+} and NO_3^- concentrations c (on log axes) in 0.5 cm sampling resolution on the respective depth scales synchronized according to Wolff et al. (2005 and personal communication). (b) Calculated records of the total depositional flux f (on log axes) of NH_4^+, Na^+ and Ca^{2+} in decadal-resolution, both shown on the EDC3 timescale.

used to check: (1) measured levels; (2) the degree of common signal variability; and (3) the robustness of the variation coefficients v_f and pairwise correlation coefficients r_f (see Section 2.2). The two cores were synchronized according to Wolff et al. (2005 and personal communication) and the outcome was confirmed with high-resolution electrolytic melt water conductivity measurements (also performed by CFA, but not shown here) and NO_3^- dips, which appear coincident with the input of volcanic acids.

Measurement levels agree well, which is obvious from the high-resolution c data (Fig. 6a) and the decadal-resolution f data (Fig. 6b), but also from calculated 200-year median values (Supplementary Fig. IIa). There are two exceptions: (1) the reversibly deposited NO_3^- (only given in Fig. 6a) which shows noticeable differences between 773 m and 780 m depth; and (2) some of the Ca^{2+} measurements around 778 m (~44.8 ka BP) and 785 m (~45.4 ka BP) depth, which were slightly distorted due to baseline fluctuations. This problem was occasionally observed in measurements from 585 m to 788 m, comprising particularly the AIM 8 event. It alters also v_f, but not r_f in this depth interval.

Apart from that, our data reveal a high degree of common signal variability within the overlap, similar to other measurements (Dielectric Profiling, Wolff et al., 2005; Barnes et al., 2006). Both, v_f and r_f, agree generally well (Supplementary Figs. IIb,c), compared to the observed range in the whole data set. Therefore, they can be used to describe decadal variability (Sections 3.4 and 3.5).

3.3. The long-term deposition flux records

The total depositional flux f of Ca^{2+} shows pronounced glacial–interglacial changes starting from equally high LGM and MIS 6 levels, but leading to distinctively lower Holocene than MIS 5.5 levels (Fig. 4, Table 1b), while c levels were similar for both (Table 1a). This leads to a factor of 18 ± 5 changes between the LGM (~18–23 ka BP) and the early Holocene (~10.0–11.5 ka BP) and 14 ± 5 between MIS 6 (~139–146 ka BP) and the early MIS 5.5 (~128–130 ka BP), respectively (Table 1b). During glacial periods strong millennial-scale Ca^{2+} variations occur in anticorrelation to the Antarctic isotope maxima (AIM) events (Röthlisberger et al.,

2002a; EPICA community members, 2006; Fischer et al., 2007b). The exclusively terrestrial nssCa^{2+} shows higher variations than Ca^{2+} with unchanged levels in cold but lower ones in warm periods (Fig. 5). Therefore, change factors (but also their errors) are further increased to 48 ± 33 and 19 ± 9, respectively (Table 1b). Additionally, reinforced millennial-scale variations can be observed within MIS 5.5 prolonged into Inception I and also in the Holocene. They are less pronounced in uncorrected Ca^{2+} (see Figs. 4 and 5) and are probably amplified through the calculation of nssCa^{2+} based on very low interglacial values of Ca^{2+} and Na^+ close to the detection limit. Thus, we refrain from discussing these short-term fluctuations as climatic signals.

Na^+ f generally reveals only moderate glacial–interglacial decreases, e.g. by a factor of 3.0 ± 0.6 from the LGM to the early Holocene, and by a factor of 4.3 ± 1.1 from MIS 6 to the early MIS 5.5 (Table 1b). It remains almost stable on maximal glacial levels (e.g. after 68 ka BP in the last and during the penultimate glacial period) with surprisingly similar LGM and MIS 6 levels and almost invisible AIM events, with the exceptions of AIM 21 and AIM 23/24. However, f levels are distinctively lower in the MIS 5.5 than in the Holocene as also observed in the EPICA Dronning Maud Land ice core (Fischer et al., 2007b), with minima during early warm periods followed by pronounced increasing trends (Fig. 4, Table 1b). Notable differences between Na^+ and the exclusively marine ssNa^+ f are observed under glacial maximum conditions (LGM, around ~65 ka BP and during MIS 6) with lower levels in ssNa^+ (Fig. 5). This leads to less pronounced glacial–interglacial f decreases by factors of 1.8 ± 0.5 and 3.0 ± 1.1, respectively (Table 1b), however, due to the source-separation calculation accompanied with larger errors.

In contrast, NH_4^+ f shows generally only very small glacial–interglacial changes, especially between the early Holocene and the LGM by a factor of only 1.1 ± 0.3, whereas it is 1.5 ± 0.4 between MIS 6 and early MIS 5.5 (Table 1b). NH_4^+ f is almost stable during glacial periods, thus AIM events are essentially invisible. LGM and MIS 6 levels are equal, whereas MIS 5.5 levels are slightly lower than Holocene ones (Fig. 4, Table 1b).

In summary, we find that the two last glacial maxima (LGM and MIS 6) appear very similar, whereas the two last interglacials (Holocene and MIS 5.5) are remarkably different, yet show a rather smooth behaviour regarding aerosol deposition. Over the two terminations, changes in f differ strongly for different aerosol species. Note that the change factors are larger for Na^+, ssNa^+ and NH_4^+ during Termination II than during Termination I, while the opposite is true for Ca^{2+} and nssCa^{2+}.

3.4. Decadal variability

Additional information to the previously discussed long-term f level changes can be gained from the high-resolution of our data, which allows for the examination of decadal variability in general or focused on singular events.

An example of such an event is shown in Fig. 3. The prominent shift in the Ca^{2+} concentration c by a factor of ~2 (and similarly in f) occurs within 1 cm at the depth of 1831.66 m around 148 ka BP. This corresponds to a mean time interval of less than 2 years according to the interpolated EDC3 timescale. It is also reflected in the NO_3^- record, as expected during dusty glacial periods, however, slightly more gradual due to post-depositional effects (see Section 3.1). Although distinctively visible in our high-resolution water-insoluble dust particle c record too (measured by a CFA laser sensor according to Lambert et al. (2008) and shown in Fig. 3), the coarse-to-fine particle ratios (derived from the same, but lower resolved size distribution measurements) do not show any concurrent significant shift. Coevally, Na^+ and NH_4^+ reveal no such signal at the same depth (Fig. 3). Similar fast shifts were so far only reported from Greenland ice cores (Steffensen et al., 2008).

To examine the general decadal variability, we calculated variation coefficients ν_f (in % according to Eq. (1) in Section 2.2) on adjacent 200-year windows over the entire homogenous decadal-resolution f records of Ca^{2+}, Na^+ and NH_4^+, allowing for comparisons between different time intervals. In contrast, the variability of the high-resolution c raw data (Fig. 2) decreases with depth due to decreasing layer thickness and data resolution. The results are shown in Fig. 7. To highlight long-term patterns, we additionally applied a low-pass filter with a 5 ka cutoff period. As seasonal signals are not preserved in the EDC ice core, it is not possible to

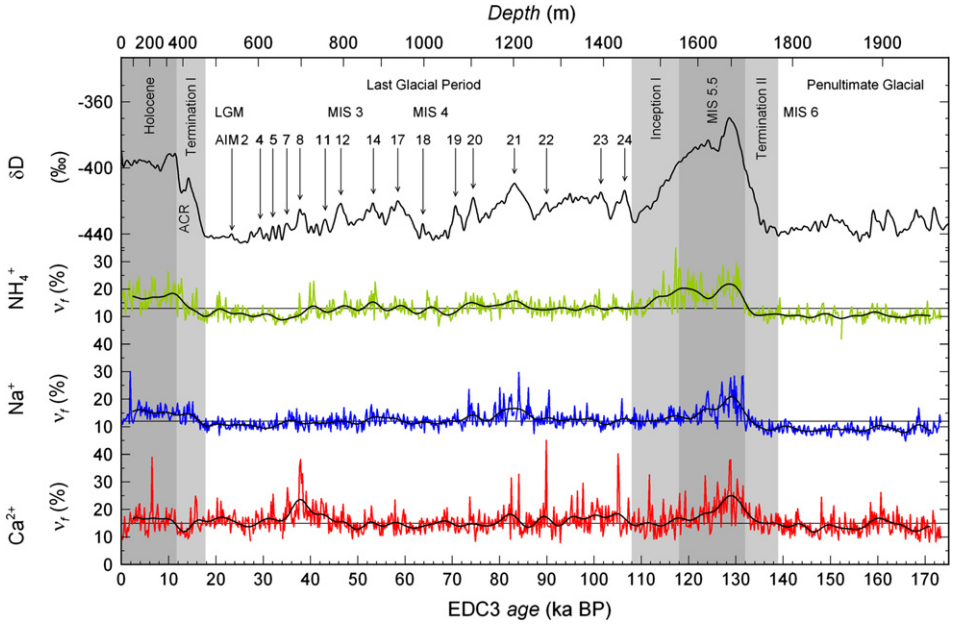

Fig. 7. Variation coefficients ν_f (thin lines) of NH_4^+, Na^+ and Ca^{2+} calculated in adjacent 200-year windows over the whole decadal-resolution flux f records. A 5 ka cutoff low-pass filter (thick black lines) was applied and the overall median value is given (thin black line, Ca^{2+} 15%, Na^+ 12%, NH_4^+ 13%) to highlight long-term variations (δD, timescale, and labels are similar to Fig. 4).

reconstruct accumulation rates in high-resolution (Legrand and Mayewski, 1997). Due to linear interpolation between given data points of the EDC3 timescale (see Section 2.3) the accumulation rate estimates are rather smooth compared to our decadal-resolution data, yielding almost similar results for both *c* and *f* records, thus there is no spurious variance introduced by this interpolation. Such behaviour can only be expected for sites with dominant dry deposition and uniform dilution of the aerosol deposition throughout the year. As we are using narrow 200-year windows to examine decadal variability, the result is furthermore not influenced by long-term variability over terminations or AIM events.

Although *f* of the different aerosol species differ markedly, the amplitudes of ν_f are rather similar for all, however slightly higher for Ca^{2+} than for Na^+ and NH_4^+, and show only moderate changes (Fig. 7). They are generally higher during interglacial periods, especially during MIS 5.5, and to a certain extent also during AIM events. The curve shape is independent from the window width chosen between 50 years and 500 years, however, overall ν_f medians of the complete records increase slightly with this parameter (for 200-year windows they are 12% for Na^+, 13% for NH_4^+ and 15% for Ca^{2+}). Due to the use of conservatively filtered decadal-resolution data we are confident to capture true atmospheric variability, not influenced by measuring errors which could play a role for data from warm periods revealing levels closer to the limit of detection; one exception is probably Ca^{2+} around AIM 8 (as discussed in Section 3.2).

3.5. Correlations of different aerosol constituents

A second approach to examine decadal variability and the interplay of different aerosol species is to calculate correlation coefficients r_f (see Section 2.2) on adjacent 200-year windows over the entire decadal-resolution log(*f*) records for Na^+ and Ca^{2+}, Ca^{2+} and NH_4^+, as well as Na^+ and NH_4^+. Note that these correlations are representative of the decadal variability in a 200-year window only, and thus are independent of long-term climatic trends, potentially resulting in covariance between the records. The results (low-pass filtered with a 5 ka cutoff period) are shown in Fig. 8. Using *c* records gives a similar result (see discussion in Section 3.4). To account for autocorrelation in the filtered data, n_{eff} (according to Eq. (2) in Section 2.2) was calculated in all 200-year intervals without gaps for each of the three different correlations. The median of each of the rather uniform series was taken yielding in one overall n_{eff} for each of the three correlations. However, the three results were very similar and moreover almost independent of the chosen maximal lag-*k* between 20 and 100. Overall we found $26 \le n_{\mathrm{eff}} \le 33$. Transferring this into an r_f value for which the positive correlation is significant on a 90% confidence level, yields $0.23 \le r_f \le 0.26$, thus roughly 0.25.

Again, amplitudes of the different r_f series appear to be rather similar at first sight. A significant positive correlation is generally found during cold glacial periods, somewhat less during AIM events. However, r_f between Na^+ and Ca^{2+} shows slightly lower positive correlations during cold glacial periods than r_f from Ca^{2+} and NH_4^+ and from Na^+ and NH_4^+, respectively. During interglacials, the correlation decreases; during MIS 5.5, it disappears even completely for all three series. Simultaneously low correlations are also found during AIM 21, whereas the situation remains ambiguous throughout the Holocene. As the parameter r_f^2 describes the proportion of the common variance shared between the two *f* series, we find maximal 60% for Na^+ and NH_4^+, 40% Ca^{2+} and NH_4^+, and 30% for Na^+ and Ca^{2+} (considering the filtered series in Fig. 8) under glacial maximum conditions.

4. Discussion

4.1. Variability and atmospheric transport

As pointed out in the introduction (Section 1.1), atmospheric transport in the southern SH has probably not changed substantially between glacial and interglacial periods. This result is supported by our *f* record of NH_4^+ (Section 3.3) which shows only very small

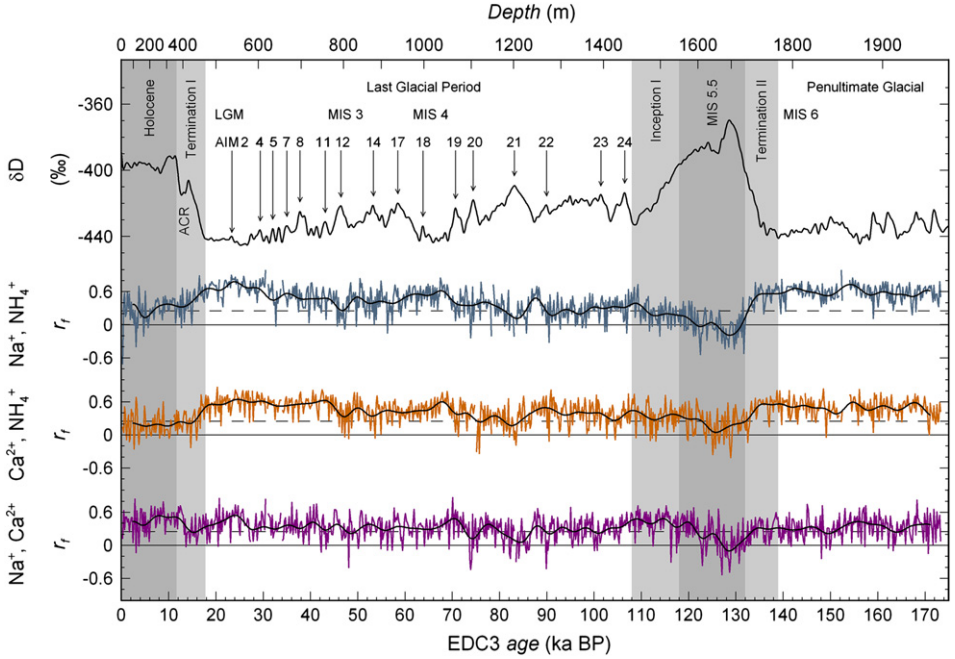

Fig. 8. Correlation coefficients r_f (thin lines) pairwise between Na^+ and NH_4^+, Ca^{2+} and NH_4^+, as well as Na^+ and Ca^{2+} calculated in adjacent 200-year windows over the whole decadal-resolution log(*f*) records. Dashed black lines are 90% confidence levels (for details see text). Additionally a 5 ka cutoff low-pass filter (thick black lines) was applied to show long-term variations (δD, timescale, and labels are similar to Fig. 4).

glacial–interglacial changes and also almost no AIM signals. Given the different amplitudes of changes, e.g. in the temperature proxy δD (Fig. 4), it is unlikely, that enhanced transport always counteracted marine bioproductivity of the SH oceans which is believed to be the only significant source for NH_4^+ deposited onto the East Antarctic plateau (Section 1.6). Thus, both transport and marine bioproductivity have not changed a lot over glacial–interglacial cycles (Kaufmann et al., 2010) as also supported by constant marine biogenic sulphate fluxes (Wolff et al., 2006).

While for $ssNa^+$ a *f* level change of a factor of ~2–3 is found during the last two terminations (Section 3.3), virtually no changes are observed over AIM events under colder glacial conditions, although there might be reasonable alterations of the source strength at the time considering, e.g. the EDC temperature proxy δD or a sea ice history from the Indian sector of the SO (Crosta et al., 2004). Fischer et al. (2007b) and Röthlisberger et al. (2008, 2010) explained the constancy on centennial timescales by the larger distance between the deposition site and the source area of $ssNa^+$ due to the larger sea ice extent (Fig. 1; Gersonde et al., 2005). Obviously, the same argument holds for decadal variations in $ssNa^+$ flux which could not be restored by those authors. Thus, the sea salt aerosol proxy becomes insensitive to source changes under colder glacial conditions, independent of whether the open ocean or the sea ice surface source is considered.

On the other hand, $nssCa^{2+}$ shows pronounced changes in *f* over glacial–interglacial cycles as well as during AIM events (Section 3.3). Although the deposition and transport seasonality is probably similar to $ssNa^+$ (Section 1.5), the $nssCa^{2+}$ source is much further away, thus co-transport is limited. Similar to previous research (Röthlisberger et al., 2002a; Wolff et al., 2006; Fischer et al., 2007a, b) we attribute $nssCa^{2+}$ *f* changes mainly to source effects. This is corroborated by events such as the observed fast and persistent shift in Ca^{2+} (and also in the dust particle flux, Section 3.4 and Fig. 3), as it is hard to explain that such an event should be a feature of atmospheric transport, that is, not reflected in other long-range transported aerosol constituents, such as Na^+ and NH_4^+, nor in the coarse-to-fine particle ratio (Section 3.4).

Despite the decidedly different glacial–interglacial flux level changes, the decadal variability of the different aerosol species is generally rather uniform around 12–15%, although slightly lower in glacial periods and higher in interglacials, especially in MIS 5.5 (Section 3.4, Fig. 7). But also the "warm" AIM 21 shows enhanced variability. This new result can be explained by processes either at the source, during atmospheric transport or deposition. Deposition effects can probably be excluded due to irreversible deposition of the considered aerosol species and prevailing dry deposition at Dome C. Source effects as well seem to play a minor role because long-term flux levels reveal huge differences while the decadal variability remains almost constant for all, Ca^{2+}, Na^+ and NH_4^+. Therefore, we assume that mainly transport effects are imprinted in the decadal variability which leads to the conclusion that transport variability was slightly higher in interglacial periods. The observed slightly decreased decadal variability during MIS 6 and LGM is in agreement with modelled similar or lower interannual variations in the transport (Lunt and Valdes, 2001) and can be explained by a northward expansion of the Antarctic vortex due to larger sea ice extent under glacial maximum conditions. As a result, storm genesis would be reduced (Watkins and Simmonds, 1995) or single storm tracks would penetrate less frequently onto the East Antarctic plateau, thus, shielding inland sites more strongly from storm intrusions compared to interglacial periods. This is in agreement with model results showing that during LGM the frequency and/or the intensity of storms did not increase in the interior of the ice sheet (Krinner and Genthon, 1998). Similar conclusions were drawn from Dome C water-insoluble particle size distribution characteristics, showing smaller particles in LGM ice samples (Delmonte et al., 2002), however, dust aerosol size distributions from other Antarctic sites show different temporal changes (Delmonte et al., 2004). A final interesting feature of the observed decadal variability is that Ca^{2+} shows generally slightly higher values than both, Na^+ and NH_4^+ (Section 3.4), presumably related to the longer transport path.

The interplay of different aerosol constituents is reflected in their pairwise correlation. Similar to the variability discussed above, correlations are as well rather uniform at first sight. However, correlation coefficients are high when variability is low and vice versa. Significant positive correlations are thus generally found during cold glacial periods with common variance up to 60% for Na^+ and NH_4^+, up to 40% Ca^{2+} and NH_4^+, and up to 30% for Na^+ and Ca^{2+} (Section 3.5, Fig. 8). It is important to bear in mind that a correlation between two variables can be attributed to either their close relationship or their simultaneous dependence on a third variable. In our context, we assume no direct relationship, as sources and maybe also the seasonality differ (Sections 1.4–1.6), but rather a dependence on an external factor. This could be either the long-range transport of the aerosols or coeval large-scale climatic influences on their sources. The high common variance related to glacial maximum conditions points to enhanced co-transport and thus a well mixed atmosphere over the East Antarctic with a predominant background aerosol at that time. This is inline with the argumentation of a more isolated Antarctic continent under glacial maximum conditions due to a northward shift of the Antarctic vortex and reduced storm genesis or frequency as mentioned above. Under such conditions transport and deposition would increasingly happen through large-scale subsidence over the East Antarctic plateau. By contrast, correlations are reduced under warmer climate conditions, e.g. during AIM 21 and the Holocene. This points to reduced isolation of the continent and a larger influence of cyclonic activity, i.e. increased storm genesis and frequency (Section 1.1) on the deposition of aerosol constituents in central East Antarctica compared to glacial maximum periods. As correlations vanish during the early MIS 5.5 this effect seems even reinforced, which is quite plausible during this significantly warmer interglacial period (Section 1.2).

Surprisingly, Na^+ and Ca^{2+} show slightly lower positive correlations than the other correlation pairs (Na and NH_4^+, Ca^{2+} and NH_4^+), although not corrected for their respective common source portions in the decadal-resolution data (see Section 2.4). Therefore, we would assume even lower correlations considering $ssNa^+$ and $nssCa^{2+}$. The reason for this observation could be the large distance between the two sources, e.g. SSA during glacial periods in the case of $nssCa^{2+}$ (Section 1.5) and for $ssNa^+$ the Indian sector of the SO (Section 1.4). Because the source of NH_4^+, our proxy for marine bioproductivity, is located within the seasonal sea ice zone and further north of the sea ice edge (Section 1.6), it shows larger correlations to both neighbouring sources, to the SSA terrestrial Ca^{2+} and even stronger to Na^+ which is also of SO origin.

Considering the decadal-resolution of our records back to the penultimate glacial period, they provide an excellent means to examine whether an Antarctic Oscillation (AAO) signal is reflected on decadal and longer time scales or not. Based on power spectra and wavelet analysis, we could, however, not pin down prominent and persistent periodic signal components in the decadal to centennial range. This is probably due to the fact that Dome C lies on the East Antarctic plateau remote from the coast, where the largest variations would be expected. Furthermore, probably more than one ice core record with appropriate data resolution is required to clearly reveal AAO signals.

4.2. Marine Isotope Stage 5.5

The importance of the Last Interglacial period MIS 5.5 with regard to paleoclimatic reconstructions is briefly described in the introduction (Section 1.2). In our records its duration spans from ~132 ka BP to ~117 ka BP (±6 ka BP; Section 2.1). A straightforward result based on our continuous decadal-resolution EDC ice core data and the very different proxies considered is that unlike, e.g. Ninnemann et al. (1999) or Bianchi and Gersonde (2002) we find no evidence for any abrupt climatic event during MIS 5.5 (Section 3.3). Moreover, there is no evidence for an Antarctic cold reversal-like event during Termination II as a counterpart of a Younger Dryas-like event found in some Northern Hemisphere records (e.g. Sánchez Goñi et al., 1999). In addition to this and the previously discussed observation of decadal variability in MIS 5.5, we discuss in the following some complementary aspects based on single proxies.

Unfortunately, nssCa^{2+} is not an unambiguous ice core proxy for SSA interglacial climate due to probably significant contributions of Australian terrestrial aerosol (Section 1.5). Therefore, we cannot attribute the higher flux levels observed during MIS 5.5 compared to the Holocene to the evolution of a specific source alone.

By contrast, ssNa^{+} is a reliable proxy for sea salt aerosol, especially during interglacial periods where it is not affected by additional errors due to the source-separation (Section 2.4) or by insensitiveness to the expansion of sea ice (Section 1.4). It is probably mainly related to the annual sea ice production rate at that time. Compared to glacial periods, the ssNa^{+} f in Dome C is lower during interglacial periods and shows minimum values during their early parts. This is in agreement with findings from marine sediment records obtained in the Atlantic sector of the SO, where early parts of interglacials exhibit low ice-rafted debris, high foraminiferal abundance, and diatom evidence indicating relatively warm sea-surface temperatures and reduced sea ice influences (Kanfoush et al., 2000, 2002; Bianchi and Gersonde, 2004). Similar effects are reported in the Indian sector of the SO (Crosta et al., 2004; Röthlisberger et al., 2010), which is rather the source region of ssNa^{+} transported to Dome C (Section 1.4). During early MIS 5.5, ssNa^{+} f is even 40% lower than in early Holocene (Table 1b), which goes along with significantly higher temperatures at Dome C (+4.5 °C, Jouzel et al., 2007). This observation points to a lower total annual sea ice production rate at that time supporting results from marine sediment cores, which reveal distinctively higher summer sea-surface temperatures (SST) and lesser diatom winter sea ice indicators for MIS 5.5 (Bianchi and Gersonde, 2002). After minimum levels at the beginning, ssNa^{+} f shows a gradual increase in the course of both interglacials, indicating a growing total annual sea ice production rate and a return to colder conditions. The same pattern is found in marine sediment cores from the Atlantic sector for both, Holocene and MIS 5.5 (Hodell et al., 2001; Bianchi and Gersonde, 2002; Kanfoush et al., 2002), and for the Indian Ocean sector (Crosta et al., 2004).

5. Conclusions

In this study we focused on decadal-resolution ice core data of aerosol constituents deposited at Dome C on the East Antarctic plateau from preindustrial Holocene back to 173 ka BP to gain insights in the climate evolution of the southern South Hemisphere beyond the Last Interglacial period MIS 5.5.

Using the accumulation rate dependent influence of post-depositional losses on NO_3^-, we were able to support the δD-derived higher accumulation rates during interglacial periods. Accumulation rate estimates are used to calculate total depositional flux records which are more representative for atmospheric concentration. In agreement with previous studies, we find that glacial–interglacial flux changes differ largely for different aerosol constituents. The terrestrial aerosol proxy nssCa^{2+}, which is related to southern South American climate during glacial periods, shows the largest changes, especially during Termination I, while the sea salt proxy ssNa^{+} changes only moderately, however more pronounced during Termination II. NH_4^+, a proxy for marine bioproductivity remains almost unchanged over glacial–interglacial cycles, especially during Termination I. Mainly based on NH_4^+, we support previous studies, which attributed large parts of the observed flux changes to the respective sources and not to changed transport conditions over glacial–interglacial cycles.

Replicated measurements on the overlap of the two EDC ice cores confirm the representativeness of variation coefficients and correlation coefficients to describe decadal variability within 200-year windows. We observed slightly lower variability and higher pairwise correlations during glacial maximum periods which is in line with only little changes in transport conditions pointing to a northward shift of the Antarctic vortex due to the larger sea ice extent and less storm activity at that time, thus, subsidence of background aerosol seems to be more important. The opposite holds for the Holocene and even more so for MIS 5.5, which shows a stronger influence of cyclonic activity on transport and deposition of aerosols at this site. However, we found no persistent periodic signal components in the decadal to centennial range.

In all examined parameters, such as flux levels, variability and pairwise correlations, we found that the LGM and the MIS 6 are very similar while the Holocene and the MIS 5.5 are different. It seems that glacial maximum conditions represent a more uniform atmospheric mode than interglacial periods. Nevertheless, our high-resolution data point to relatively smooth climatic conditions during the MIS 5.5 interglacial period without any abrupt climatic events. At that time, and in agreement with marine sediment records, ssNa^{+} seems to be a reliable proxy for total annual sea ice production rate in the adjacent Indian sector of the Southern Ocean, showing distinct minima during early Holocene and even 40% lower during early MIS 5.5, in both cases followed by a pronounced increasing trend. In contrast, it would be interesting to correlate our nssCa^{2+} record, which seems to be a reliable proxy for SSA glacial climate, to proxy records derived directly from this area, especially for time periods beyond the LGM, however, such data are currently scarce (Kaplan et al., 2008).

Acknowledgements

This work is a contribution to the European Project for Ice Coring in Antarctica (EPICA), a joint European Science Foundation/European Commission (EC) scientific programme, funded by the EU (EPICA-MIS) and by national contributions from Belgium, Denmark, France, Germany, Italy, The Netherlands, Norway, Sweden, Switzerland and the UK. The main logistic support at Dome C was provided by IPEV and PNRA. We thank all the persons involved in the fieldwork to obtain the comprehensive data set.

Appendix A. Supplemental material

Supplementary information for this manuscript can be downloaded at doi:10.1016/j.quascirev.2009.09.009.

References

Barnes, P.R.F., Wolff, E.W., Mulvaney, R., 2006. A 44 kyr paleoroughness record of the Antarctic surface. Journal of Geophysical Research 111, D03102.

Bianchi, C., Gersonde, R., 2002. The Southern Ocean surface between Marine Isotope Stages 6 and 5d: shape and timing of climate changes. Palaeogeography, Palaeoclimatology, Palaeoecology 187, 151–177.

Bianchi, C., Gersonde, R., 2004. Climate evolution at the last deglaciation: the role of the Southern Ocean. Earth and Planetary Science Letters 228, 407–424.

Bigler, M., Röthlisberger, R., Lambert, F., Stocker, T.F., Wagenbach, D., 2006. Aerosol deposited in East Antarctica, over the last glacial cycle: detailed apportionment of continental and sea salt contributions. Journal of Geophysical Research – Atmospheres 111, D08205.

Bowen, H.J.M., 1979. Environmental Chemistry of the Elements. Academic Press, London.

Broecker, W.S., Henderson, G.M., 1998. The sequence of events surrounding termination II and their implications for the cause of glacial–interglacial CO2 changes. Paleoceanography 13, 352–364.

Castellano, E., Becagli, S., Jouzel, J., Migliori, A., Severi, M., Steffensen, J.P., Traversi, R., Udisti, R., 2004. Volcanic eruption frequency over the last 45 ky as recorded in Epica-Dome C ice core (East Antarctica) and its relationship with climatic changes. Global and Planetary Change 42, 195–205.

Cosme, E., Hourdin, F., Genthon, C., Martinerie, P., 2005. Origin of dimethylsulfide, non-sea-salt sulfate, and methanesulfonic acid in eastern Antarctica. Journal of Geophysical Research 110, D03302.

Crosta, X., Sturm, A., Armand, L., Pichon, J.J., 2004. Late Quaternary sea ice history in the Indian sector of the Southern Ocean as recorded by diatom assemblages. Marine Micropaleontology 50, 209–223.

Delmonte, B., Petit, J.R., Maggi, V., 2002. Glacial to Holocene implications of the new 27000-year dust record from the EPICA Dome C (East Antarctica) ice core. Climate Dynamics 18, 647–660.

Delmonte, B., Petit, J.R., Andersen, K.K., Basile-Doelsch, I., Maggi, V., Ya Lipenkov, V., 2004. Dust size evidence for opposite regional atmospheric circulation changes over east Antarctica during the last climatic transition. Climate Dynamics 23, 427–438.

Delmonte, B., Andersson, P.S., Hansson, M., Schöberg, H., Petit, J.R., Basile-Doelsch, I., Maggi, V., 2008. Aeolian dust in East Antarctica (EPICA-Dome C and Vostok): provenance during glacial ages over the last 800 kyr. Geophysical Research Letters 35, L07703.

Delmonte, B., Andersson, P.S., Schöberg, H., Hansson, M., Petit, J.R., Delmas, R., Gaiero, D.M., Maggi, V., Frezzotti, M., 2010. Geographic provenance of aeolian dust in East Antarctica during Pleistocene glaciations: preliminary results from Talos Dome and comparison with East Antarctic and new Andean ice core data. Quaternary Science Reviews 29, 256–264.

EPICA community members, 2004. Eight glacial cycles from an Antarctic ice core. Nature 429, 623–628.

EPICA community members, 2006. One-to-one coupling of glacial climate variability in Greenland and Antarctica. Nature 444, 195–198.

Fischer, H., Siggaard-Andersen, M.-L., Ruth, U., Röthlisberger, R., Wolff, E., 2007a. Glacial/interglacial changes in mineral dust and sea-salt records in polar ice cores: sources, transport, and deposition. Reviews of Geophysics 45 RG1002.

Fischer, H., Fundel, F., Ruth, U., Twarloh, B., Wegner, A., Udisti, R., Becagli, S., Castellano, E., Morganti, A., Severi, M., Wolff, E., Littot, G., Röthlisberger, R., Mulvaney, R., Hutterli, M.A., Kaufmann, P., Federer, U., Lambert, F., Bigler, M., Hansson, M., Jonsell, U., de Angelis, M., Boutron, C., Siggaard-Andersen, M.-L., Steffensen, J.P., Barbante, C., Gaspari, V., Gabrielli, P., Wagenbach, D., 2007b. Reconstruction of millennial changes in dust emission, transport and regional sea ice coverage using the deep EPICA ice cores from the Atlantic and Indian Ocean sector of Antarctica. Earth and Planetary Science Letters 260, 340–354.

Gaiero, D.M., 2007. Dust provenance in Antarctic ice during glacial periods: from where in southern South America? Geophysical Research Letters 34, L17707.

Gersonde, R., Crosta, X., Abelmann, A., Armand, L., 2005. Sea-surface temperature and sea ice distribution of the Southern Ocean at the EPILOG Last Glacial Maximum – a circum-Antarctic view based on siliceous microfossil records. Quaternary Science Reviews 24, 869–896.

Gibbard, P.L., 2003. Definition of the Middle-Upper Pleistocene boundary. Global and Planetary Change 36, 201–208.

Hara, K., Osada, K., Kido, M., Hayashi, M., Matsunaga, K., Iwasaka, Y., Yamanouchi, T., Hashida, G., Fukatsu, T., 2004. Chemistry of sea-salt particles and inorganic halogen species in Antarctic regions: compositional differences between coastal and inland stations. Journal of Geophysical Research-Atmospheres 109.

Hodell, D.A., Kanfoush, S.L., Shemesh, A., Crosta, X., Charles, C.D., Guilderson, T.P., 2001. Abrupt cooling of Antarctic surface waters and sea ice expansion in the South Atlantic sector of the Southern Ocean at 5000 cal yr B.P. Quaternary Research 56, 191–198.

Huybrechts, P., 2009. Cryosphere. In: Gornitz, V. (Ed.), Encyclopedia of Paleoclimatology and Ancient Environments. Springer, Dordrecht, The Netherlands, pp. 221–225.

Iriondo, M., 2000. Patagonian dust in Antarctica. Quaternary International 68, 83–86.

Jansen, E., Overpeck, J., Briffa, K.R., Duplessy, J.-C., Joos, F., Masson-Delmotte, V., Olago, D., Otto-Bliesner, B., Peltier, W.R., Rahmstorf, S., Ramesh, R., Raynaud, D., Rind, D., Solomina, O., Villalba, R., Zhang, D., 2007. Paleoclimate. In: Solomon, S., Qin, D., Manning, M., Chen, Z., Marquis, M., Averyt, K.B., Tignor, M., Miller, H.L. (Eds.), Climate Change 2007: The Physical Science Basis. Contribution of Working group I to the Fourth Assessment Report of the Intergovernmental Panel on Climate Change. Cambridge University Press, United Kingdom and New York, NY, USA, pp. 433–497. Cambridge.

Johnson, M.T., Bell, T.G., 2008. Coupling between dimethylsulfide emissions and the ocean-atmosphere exchange of ammonia. Environmental Chemistry 5, 259–267.

Jourdain, B., Preunkert, S., Cerri, O., Castebrunet, H., Udisti, R., Legrand, M., 2008. Year-round record of size-segregated aerosol composition in central Antarctica (Concordia station): implications for the degree of fractionation of sea-salt particle. Journal of Geophysical Research, 113, D14308.

Jouzel, J., Masson-Delmotte, V., Cattani, O., Dreyfus, G., Falourd, S., Hoffmann, G., Minster, B., Nouet, J., Barnola, J.M., Chappellaz, J., Fischer, H., Gallet, J.C., Johnsen, S., Leuenberger, M., Loulergue, L., Luethi, D., Oerter, H., Parrenin, F., Raisbeck, G., Raynaud, D., Schilt, A., Schwander, J., Selmo, E., Souchez, R., Spahni, R., Stauffer, B., Steffensen, J.P., Stenni, B., Stocker, T.F., Tison, J.L., Werner, M., Wolff, E.W., 2007. Orbital and millennial Antarctic climate variability over the past 800,000 years. Science 317, 793–796.

Kanfoush, S.L., Hodell, D.A., Charles, C.D., Guilderson, T.P., Mortyn, P.G., Ninnemann, U.S., 2000. Millennial-scale instability of the Antarctic Ice Sheet during the last glaciation. Science 288, 1815–1818.

Kanfoush, S.L., Hodell, D.A., Charles, C.D., Janecek, T.R., Rack, F.R., 2002. Comparison of ice-rafted debris and physical properties in ODP Site 1094 (South Atlantic) with the Vostok ice core over the last four climatic cycles. Palaeogeography Palaeoclimatology Palaeoecology 182, 329–349.

Kaplan, M.R., Moreno, P.I., Rojas, M., 2008. Glacial dynamics in southernmost South America during Marine Isotope Stage 5e to the Younger Dryas chron: a brief review with a focus on cosmogenic nuclide measurements. Journal of Quaternary Science 23, 649–658.

Kaufmann, P.R., Federer, U., Hutterli, M.A., Bigler, M., Schüpbach, S., Ruth, U., Schmitt, J., Stocker, T.F., 2008. An improved continuous flow analysis system for high-resolution field measurements on ice cores. Environmental Science and Technology 42, 8044–8050.

Kaufmann, P., Fundel, F., Fischer, H., Bigler, M., Ruth, U., Udisti, R., Hansson, M., de Angelis, M., Barbante, C., Wolff, E.W., Hutterli, M., Wagenbach, D., 2010. Ammonium and non-sea-salt sulphate in the EPICA ice cores as indicator of biological activity in the Southern Ocean. Quaternary Science Reviews 29, 313–323.

King, J.C., Turner, J., 1997. Antarctic Meteorology and Climatology. Cambridge University Press, Cambridge, UK.

Krinner, G., Genthon, C., 1998. GCM simulations of the Last Glacial Maximum surface climate of Greenland and Antarctica. Climate Dynamics 14, 741–758.

Krinner, G., Genthon, C., 2003. Tropospheric transport of continental tracers towards Antarctica under varying climatic conditions. Tellus 55B, 54–70.

Lambert, F., Delmonte, B., Petit, J.R., Bigler, M., Kaufmann, P.R., Hutterli, M.A., Stocker, T.F., Ruth, U., Steffensen, J.P., Maggi, V., 2008. Dust-climate couplings over the past 800,000 years from the EPICA Dome C ice core. Nature 452, 616–619.

Legrand, M., 1987. Chemistry of Antarctic snow and ice. Journal De Physique 48, 77–86.

Legrand, M., Mayewski, P., 1997. Glaciochemistry of polar ice cores: a review. Reviews of Geophysics 35, 219–243.

Legrand, M., Ducroz, F., Wagenbach, D., Mulvaney, R., Hall, J., 1998. Ammonium in coastal Antarctic aerosol and snow: role of polar ocean and penguin emission. Journal of Geophysical Research 103, 11,043–11,056.

Legrand, M., Wagenbach, D., Jourdain, B., 1999. Origins of ammonium in Antarctic air and snow deposits. Eos Transactions. American Geophysical Union 80, 198.

Li, F., Ginoux, P., Ramaswamy, V., 2008. Distribution, transport, and deposition of mineral dust in the Southern Ocean and Antarctica: contribution of major sources. Journal of Geophysical Research 113, D10207.

Littot, G.C., Mulvaney, R., Röthlisberger, R., Udisti, R., Wolff, E.W., Castellano, E., de Angelis, M., Hansson, M.E., Sommer, S., Steffensen, J.P., 2002. Comparison of analytical methods used for measuring major ions in the EPICA Dome C (Antarctica) ice core. Annals of Glaciology 35, 299–305.

Loutre, M.F., Berger, A., 2003. Marine Isotope Stage 11 as an analogue for the present interglacial. Global and Planetary Change 36, 209–217.

Lunt, D.J., Valdes, P.J., 2001. Dust transport to Dome C, Antarctica at the Last Glacial Maximum and present day. Geophysical Research Letters 28, 295–298.

Ninnemann, U.S., Charles, C.D., Hodell, D.A., 1999. Origin of global millennial scale climate events: constraints from the southern ocean deep sea sedimentary record. In: Webb, R.S., Clark, P.U., Keigwin, L.D. (Eds.), Mechanisms of Global Climate Change at Millennial Time Scales. American Geophysical Union, p. 394.

Overpeck, J.T., Otto-Bliesner, B.L., Miller, G.H., Muhs, D.R., Alley, R.B., Kiehl, J.T., 2006. Paleoclimatic evidence for future ice-sheet instability and rapid sea-level rise. Science 311, 1747–1750.

Parrenin, F., Dreyfus, G., Durand, G., Fujita, S., Gagliardini, O., Gillet, F., Jouzel, J., Kawamura, K., Lhomme, N., Masson-Delmotte, V., Ritz, C., Schwander, J., Shoji, H., Uemura, R., Watanabe, O., Yoshida, N., 2007a. 1-D-ice flow modelling at EPICA Dome C and Dome Fuji, East Antarctica. Climate of the Past 3, 243–259.

Parrenin, F., Barnola, J.-M., Beer, J., Blunier, T., Castellano, E., Chappellaz, J., Dreyfus, G., Fischer, H., Fujita, S., Jouzel, J., Kawamura, K., Lemieux-Dudon, B., Loulergue, L., Masson-Delmotte, V., Narcisi, B., Petit, J.-R., Raisbeck, G., Raynaud, D., Ruth, U., Schwander, J., Severi, M., Spahni, R., Steffensen, J.P., Svensson, A., Udisti, R., Waelbroeck, C., Wolff, E., 2007b. The EDC3 chronology for the EPICA Dome C ice core. Climate of the Past 3, 485–497.

Quenouille, M.H., 1952. Associated Measurements. Butterworth, London.

Rankin, A.M., Auld, V., Wolff, E.W., 2000. Frost flowers as a source of fractionated sea salt aerosol in the polar regions. Geophysical Research Letters 27, 3469–3472.

Rao, V.B., Alexandre, M.C.d.C., Sergio, H.F., 2003. Interannual variations of storm tracks in the Southern Hemisphere and their connections with the Antarctic oscillation. International Journal of Climatology 23, 1537–1545.

Reijmer, C.H., van den Broeke, M.R., Scheele, M.P., 2002. Air parcel trajectories and snowfall related to five deep drilling locations in Antarctica based on the ERA-15 dataset. Journal of Climate 15, 1957–1968.

Revel-Rolland, M., De Deckker, P., Delmonte, B., Hesse, P.P., Magee, J.W., Basile-Doelsch, I., Grousset, F., Bosch, D., 2006. Eastern Australia: a possible source of dust in East Antarctica interglacial ice. Earth and Planetary Science Letters 249, 1–13.

Röthlisberger, R., Hutterli, M.A., Sommer, S., Wolff, E.W., Mulvaney, R., 2000a. Factors controlling nitrate in ice cores: evidence from the Dome C deep ice core. Journal of Geophysical Research 105, 20,565–20,573.

Röthlisberger, R., Bigler, M., Hutterli, M., Sommer, S., Stauffer, B., Junghans, H.G., Wagenbach, D., 2000b. Technique for continuous high-resolution analysis of trace substances in firn and ice cores. Environmental Science and Technology 34, 338–342.

Röthlisberger, R., Mulvaney, R., Wolff, E.W., Hutterli, M.A., Bigler, M., Sommer, S., Jouzel, J., 2002a. Dust and sea salt variability in central East Antarctica (Dome C) over the last 45 kyrs and its implications for southern high-latitude climate. Geophysical Research Letters 29, 1963.

Röthlisberger, R., Hutterli, M.A., Wolff, E.W., Mulvaney, R., Fischer, H., Bigler, M., Goto-Azuma, K., Hansson, M.E., Ruth, U., Siggaard-Andersen, M.-L., Steffensen, J.P., 2002b. Nitrate in Greenland and Antarctic ice cores: a detailed description of post-depositional processes. Annals of Glaciology 35, 209–216.

Röthlisberger, R., Mudelsee, M., Bigler, M., de Angelis, M., Fischer, H., Hansson, M., Lambert, F., Masson-Delmotte, V., Sime, L., Udisti, R., Wolff, E.W., 2008. The Southern Hemisphere at glacial terminations: insights from the Dome C ice core. Climate of the Past 4, 345–356.

Röthlisberger, R., Crosta, X., Abram, N.J., Armand, L., Wolff, E.W., 2010. Potential and limitations of marine and ice core sea ice proxies: an example from the Indian Ocean sector. Quaternary Science Reviews 29, 296–302.

Sánchez Goñi, M.F., Eynaud, F., Turon, J.L., Shackleton, N.J., 1999. High resolution palynological record off the Iberian margin: direct land-sea correlation for the Last Interglacial complex. Earth and Planetary Science Letters 171, 123–137.

Schwander, J., Jouzel, J., Hammer, C.U., Petit, J.-R., Udisti, R., Wolff, E., 2001. A tentative chronology for the EPICA Dome Concordia ice core. Geophysical Research Letters 28, 4243–4246.

Shulmeister, J., Goodwin, I., Renwick, J., Harle, K., Armand, L., McGlone, M.S., Cook, E., Dodson, J., Hesse, P.P., Mayewski, P., Curran, M., 2004. The Southern Hemisphere westerlies in the Australasian sector over the last glacial cycle: a synthesis. Quaternary International 118-19, 23–53.

Silvente, E., Legrand, M., 1993. Ammonium to sulphate ratio in aerosol and snow of Greenland and Antarctic Regions. Geophysical Research Letters 20, 687–690.

Simmonds, I., 2003. Modes of atmospheric variability over the Southern Ocean. Journal of Geophysical Research-Oceans 108, 8078.

Sommer, S., Wagenbach, D., Mulvaney, R., Fischer, H., 2000. Glacio-chemical study spanning the past 2 kyr on three ice cores from Dronning Maud Land, Antarctica. 2. Seasonally resolved chemical records. Journal of Geophysical Research 105, 29,423–29,433.

Steffensen, J.P., Andersen, K.K., Bigler, M., Clausen, H.B., Dahl-Jensen, D., Fischer, H., Goto-Azuma, K., Hansson, M., Johnsen, S.J., Jouzel, J., Masson-Delmotte, V., Popp, T., Rasmussen, S.O., Röthlisberger, R., Ruth, U., Stauffer, B., Siggaard-Andersen, M.-L., Sveinbjornsdottir, A.E., Svensson, A., White, J.W.C., 2008. High-resolution Greenland ice core data show abrupt climate change happens in few years. Science 321, 680–684.

Stirling, C.H., Esat, T.M., Lambeck, K., McCulloch, M.T., 1998. Timing and duration of the Last Interglacial: evidence for a restricted interval of widespread coral reef growth. Earth and Planetary Science Letters 160, 745–762.

Sugden, D.E., McCulloch, R.D., Bory, A.J.M., Hein, A.S., 2009. Influence of Patagonian glaciers on Antarctic dust deposition during the last glacial period. Nature Geoscience 2, 281–285.

Thompson, D.W.J., Wallace, J.M., 2000. Annular modes in the extratropical circulation Part I: month-to-month variability. Journal of Climate 13, 1000–1016.

Udisti, R., Becagli, S., Castellano, E., Delmonte, B., Jouzel, J., Petit, J.R., Schwander, J., Stenni, B., Wolff, E.W., 2004. Stratigraphic correlations between the European Project for Ice Coring in Antarctica (EPICA) Dome C and Vostok ice cores showing the relative variations of snow accumulation over the past 45 kyr. Journal of Geophysical Research 109.

van Kolfschoten, T., Gibbard, P.L., Knudsen, K.-L., 2003. The Eemian interglacial: a global perspective. Introduction. Global and Planetary Change 36, 147–149.

Wagenbach, D., Ducroz, F., Mulvaney, R., Keck, L., Minikin, A., Legrand, M., Hall, J.S., Wolff, E.W., 1998. Sea-salt aerosol in coastal Antarctic regions. Journal of Geophysical Research 103, 10,961–10,974.

Watkins, A.B., Simmonds, I., 1995. Sensitivity of numerical prognoses to Antarctic sea ice distribution. Journal of Geophysical Research 100, 22,681–22,696.

Weller, R., Wagenbach, D., 2007. Year-round chemical aerosol records in continental Antarctica obtained by automatic samplings. Tellus B 59, 755–765.

Whitlow, S., Mayewski, P.A., Dibb, J.E., 1992. A comparison of major chemical species seasonal concentration and accumulation at the South Pole and summit, Greenland. Atmospheric Environment. Part A. General Topics 26, 2045–2054.

Wolff, E.W., Rankin, A.M., Röthlisberger, R., 2003. An ice core indicator of Antarctic sea ice production? Geophysical Research Letters 30.

Wolff, E.W., Cook, E., Barnes, P.R.F., Mulvaney, R., 2005. Signal variability in replicate ice cores. Journal of Glaciology 51, 462–468.

Wolff, E.W., Fischer, H., Fundel, F., Ruth, U., Twarloh, B., Littot, G.C., Mulvaney, R., Röthlisberger, R., de Angelis, M., Boutron, C.F., Hansson, M., Jonsell, U., Hutterli, M.A., Lambert, F., Kaufmann, P., Stauffer, B., Stocker, T.F., Steffensen, J.P., Bigler, M., Siggaard-Andersen, M.L., Udisti, R., Becagli, S., Castellano, E., Severi, M., Wagenbach, D., Barbante, C., Gabrielli, P., Gaspari, V., 2006. Southern Ocean sea-ice extent, productivity and iron flux over the past eight glacial cycles. Nature 440, 491–496.

Wolff, E.W., Jones, A.E., Bauguitte, S.J.B., Salmon, R.A., 2008. The interpretation of spikes and trends in concentration of nitrate in polar ice cores, based on evidence from snow and atmospheric measurements. Atmospheric Chemistry and Physics 8, 5627–5634.

Wolff, E.W., Barbante, C., Becagli, S., Bigler, M., Boutron, C.F., Castellano, E., de Angelis, M., Federer, U., Fischer, H., Fundel, F., Hansson, M., Hutterli, M., Jonsell, U., Karlin, T., Kaufmann, P., Lambert, F., Littot, G.C., Mulvaney, R., Röthlisberger, R., Ruth, U., Severi, M., Siggaard-Andersen, M.L., Sime, L.C., Steffensen, J.P., Stocker, T.F., Traversi, R., Twarloh, B., Udisti, R., Wagenbach, D., Wegner, A., 2010. Changes in environment over the last 800,000 years from chemical analysis of the EPICA Dome C ice core. Quaternary Science Reviews 29, 285–295.

Yang, X., Pyle, J.A., Cox, R.A., 2008. Sea salt aerosol production and bromine release: role of snow on sea ice. Geophysical Research Letters 35, L16815.

Yiou, P., Fuhrer, K., Meeker, L.D., Jouzel, J., Johnson, S., Mayewski, P.A., 1997. Paleoclimatic variability inferred from the spectral analysis of Greenland and Antarctic ice-core data. Journal of Geophysical Research 102, 26441–26454.